Available online at www.sciencedirect.com
SCIENCE DIRECT
Biochimica et Biophysica Acta 1712 (2005) 173 – 184
BIOCHIMICA ET BIOPHYSICA ACTA
BBA
http://www.elsevier.com/locate/bba

Membrane topology of loop 13–14 of the Na^+/glucose cotransporter (SGLT1): A SCAM and fluorescent labelling study

Dominique G. Gagnon, Andrea Holt, Francis Bourgeois, Bernadette Wallendorff, Michael J. Coady, Jean-Yves Lapointe*

Groupe d'étude des protéines membranaires (GÉPROM), Université de Montréal, C.P. 6128, succ. centre-ville, Montréal, Québec, Canada H3C 3J7

Received 11 February 2005; received in revised form 29 March 2005; accepted 18 April 2005
Available online 4 May 2005

Abstract

The accessibility of the hydrophilic loop between putative transmembrane segments XIII and XIV of the Na^+/glucose cotransporter (SGLT1) was studied in *Xenopus* oocytes, using the substituted cysteine accessibility method (SCAM) and fluorescent labelling. Fifteen cysteine mutants between positions 565 and 664 yielded cotransport currents of similar amplitude than the wild-type SGLT1 (wtSGLT1). Extracellular, membrane-impermeant $MTSES^{(-)}$ and $MTSET^{(+)}$ had no effect on either cotransport or Na^+ leak currents of wtSGLT1 but 9 mutants were affected by MTSES and/or MTSET. We also performed fluorescent labelling on SGLT1 mutants, using tetramethylrhodamine-5-maleimide and showed that positions 586, 588 and 624 were accessible. As amino acids 604 to 610 in SGLT1 have been proposed to form part of a phlorizin (Pz) binding site, we measured the K_i^{Pz} and $K_m^{\alpha MG}$ for wtSGLT1 and for cysteine mutants at positions 588, 605–608 and 625. Although mutants A605C, Y606C and D607C had slightly higher K_i^{Pz} values than wtSGLT1 with minimal changes in $K_m^{\alpha MG}$, the effects were modest and do not support the original hypothesis. We conclude that the large, hydrophilic loop near the carboxyl terminus of SGLT1 is thus accessible to the external solution but does not appear to play a major part in the binding of phlorizin.

Keywords: Na^+/glucose cotransporter; Electrophysiology; SCAM; Fluorescence; Topology

1. Introduction

Despite their important physiological roles, little is known about the three-dimensional structures of membrane proteins and less than 35 different protein folds have been reported for transporters, channels or pumps (http://www.blanco.biomol.uci.edu/Membrane_Proteins_xtal.html). In the absence of physical structure, an important step in our understanding of their mechanisms of action at the molecular level is to correctly identify the orientation of each protein segment with respect to the membrane. In the case of the Na^+/glucose cotransporter SGLT1[1], an archetype for Na^+ cotransporters, a proposed membrane topology posits extracellular N- and C-termini and 14 transmembrane segments (TMS) [1] comprising 48% of the protein. This model is based on hydrophobicity plots and on the insertion of glycosylation sites at different locations along the protein.

Several studies employing site-directed mutagenesis and chimeric constructions of SGLT1 have sought to identify the amino acids forming the Na^+ binding sites, the glucose binding site and the voltage sensor responsible for the charge displacement observed in the absence of glucose. Since expression of a truncated protein composed of TMS 10–13 of

Abbreviations: SGLT1, high affinity Na^+/glucose cotransporter; hSGLT1, human isoform of SGLT1; rSGLT1, rabbit isoform of SGLT1; wtSGLT1, wild-type SGLT1; SCAM, substituted cysteine accessibility method; MTS, methanethiosulfonate; MTSES, sodium (2-sulfonatoethyl)-methanethiosulfonate; MTSET, [2-(Trimethylammonium) ethyl]-methanethiosulfonate bromide; MTSEA, 2-aminoethyl methanethiosulfonate hydrobromide; TMR5(6)M, tetramethylrhodamine-5(or 6)-maleimide; TMS, transmembrane segment; Pz, phlorizin; αMG, α−Methyl-glucose; V_m, membrane potential; I_{cotr}, αMG cotransport current; I_{leak}, Na^+ leak current; AA, amino acid; $K_m^{\alpha MG}$, apparent affinity for αMG; K_i^{Pz}, inhibition constant of Pz; K_m^{Na+}, apparent affinity for Na^+; VSVG, vesicular stomatitis virus G protein

* Corresponding author. Tel.: +1 514 343 7046; fax: +1 514 343 7146.
E-mail address: jean-yves.lapointe@umontreal.ca (J.-Y. Lapointe).

0005-2736/$ - see front matter © 2005 Elsevier B.V. All rights reserved.
doi:10.1016/j.bbamem.2005.04.007

SGLT1 in *Xenopus* oocytes is associated with an increase in glucose permeability, it has been suggested that the C-terminal end of SGLT1 forms the glucose permeation pathway [2,3]. However, this permeation pathway does not appear to be specific for glucose as mannitol fluxes were also increased and Pz sensitivity was lost [3]. Replacing residue Q457 with a cysteine in this C-terminal portion of SGLT1 and labelling it with a fluorophore (tetramethylrhodamine-6-maleimide, TMR6M) showed that this residue is involved in a voltage-dependent conformational change that affects the fluorescence of TMR6M by 4–5% [4,5]. The putative loop between TMS 4 and 5 has been proposed to form part of the Na^+ interaction and voltage sensing domain based on an interpretation of the effects on pre-steady state currents of mutation of a series of amino acids there to cysteine residues +/− thiol-binding reagents [6–9]. The evidence supporting the physical separation between the putative pathways used by Na^+ and glucose appears questionable especially when compared to the recent crystallographic structure of the H^+/lactose cotransporter [10].

An extremely hydrophilic segment of 88 amino acids positioned between the 13th and 14th TMS (amino acids (AA) #549 to 637 in the human clone) is considered to be intracellular by the model described above. This region is also noteworthy because it contains a quite conserved sequence followed by a less conserved one when the SGLT1 protein sequence is aligned with the closely related SGLT2 and SGLT3 proteins (see Fig. 1A). The location of this segment, which contains 37 charged amino acids (21 negatively charged and 16 positively charged), was later challenged by Kinne's group based on the observation that histidine tags inserted at positions 584–588 and 622–627 can be recognized by an antibody in the external solution [11]. More recently, the segment between 604 and 610 has also been proposed to be involved in the extracellular binding site for phlorizin (Pz), a specific inhibitor for SGLT1 [12–14].

As a step in establishing the structure and function of loop 13–14, we report here our observations of the electrophysiological characterization and fluorescent labelling of 15 different cysteine mutants created between residues N565 and A664 within the last hydrophilic loop and the last TMS of human SGLT1 expressed in *Xenopus* oocytes. The results clearly indicate that at least 10 of these 15 mutants are accessible from the extracellular solution by membrane-impermeant reagents or with a rhodamine-based fluorophore (tetramethylrhodamine-5-maleimide, TMR5M). In addition, mutations at positions 605–608 suggest a weak role for this segment in the ability of SGLT1 to bind extracellular Pz.

2. Materials and methods

2.1. Molecular biology

We used human SGLT1 cDNA with an N-terminal myc epitope in the expression vector pBS (pBS-myc-hSGLT1) [15] to construct each of the mutations described here. They were created using the method described by Fisher and Pei [16]. Individual mutations were confirmed by DNA sequencing and the specific amino acids which were mutated to cysteine are indicated in Fig. 1B. QIAGEN mini-prep kits were used to extract DNA and *Eco*RI digestion was followed by mRNA transcription in vitro using the T3 mMessage mMachine kit (Ambion, Austin TX).

2.2. Oocyte preparation and injection

Oocytes were surgically removed from *Xenopus laevis* frogs, dissected and defolliculated as described previously [15,17]. They were injected with 46 nl mRNA (0.25 μg/μl), aside from the wild-type SGLT1 (wtSGLT1), which was injected with 46 nl of a 0.1 μg/μl solution, and maintained in Barth's solution (in mM: 90 NaCl, 3 KCl, 0.82 $MgSO_4$, 0.41 $CaCl_2$, 0.33 $Ca(NO_3)_2$, 5 HEPES, pH 7.6) supplemented with 5% horse serum, 2.5 mM Na^+ pyruvate, 100 U/ml penicillin and 0.1 mg/ml streptomycin for 4–8 days prior to experimental use.

2.3. Electrophysiology

The saline solution is composed of (in mM): 90 NaCl, 3 KCl, 0.82 $MgCl_2$, 0.74 $CaCl_2$, 10 HEPES, and the solution pH was adjusted to 7.6 with NaOH. Steady-state currents were measured with 5 mM α-Methyl-glucose (αMG) and 200 μM phlorizin (Pz) for all experiments except for determination of apparent affinity for αMG ($K_m^{\alpha MG}$) and inhibition constant of Pz (K_i^{Pz}), which were done as described previously [15]. Two-microelectrode voltage clamp experiments were performed with an Oocyte Clamp OC-725 (Warner Instrument Corp, Hamden, CT). Three repetitions of membrane potential steps (25 mV or 20 mV) between + 70 and −170 mV were imposed for 300 ms intervals per step. Data were obtained with a sampling frequency of 10 kHz (V was filtered at 1 kHz lowpass), and the 3 repetitions were averaged during the experiment by the acquisition program (Clampex 8.2.0.228, Axon Instruments Inc, Union City, CA). Steady-state current levels were obtained using mean values for measurements at the end of each pulse (between 150 and 300 ms). Treatments with 2.5 mM methanethiosulfonate (MTS) reagents were performed at the normal holding potential (−50 mV) in a saline solution for 5 to 10 min; afterwards, the bath was washed sufficiently to eliminate unbound reactants. The activity of the cotransporter was tested before and after the treatment. The effects of treatments on the different mutants were normalized by dividing currents measured after treatment with the currents measured before treatment; these were compared to wtSGLT1 currents, normalized in the same fashion.

2.4. Fluorescence

A Nikon Diaphot inverted microscope was employed with a 40× oil immersion objective (numerical aperture

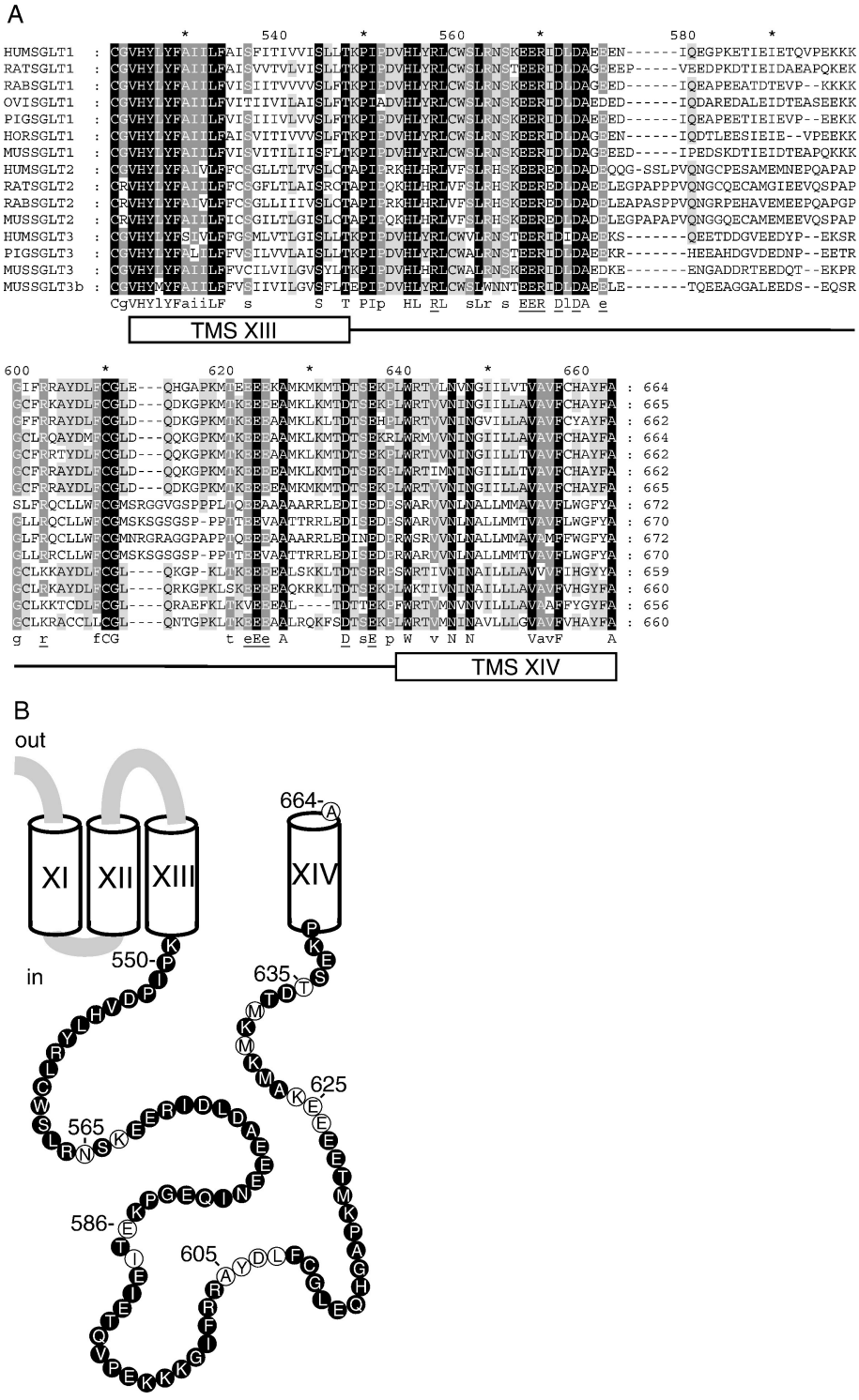

Fig. 1. Properties and topology of loop 13–14 of the Na^+/glucose cotransporter. (A) Sequence alignment of some isoforms of SGLT1, SGLT2 and SGLT3 between amino acids 540 and 664. Black columns represent 100% amino acid conservation, dark grey and light grey represent 80% and 60% conservation, respectively. The first line indicates the position in the amino acid sequence of hSGLT1 and the last line is the consensus sequence. Boxes depict the purported TMS regions. (B) A current topological model of the last 4 transmembrane segments of the cotransporter. TMS are identified by Roman numerals, some amino acid positions in the protein sequence are indicated, the amino acids which were mutated to cysteine in the present study are depicted in white circles and the extracellular and intracellular side are indicated by the words “out” and “in”, respectively.

1.30, Nikon, Tokyo, Japan). A Lambda LS 175 W xenon arc lamp connected to a liquid light guide was used to illuminate oocytes (Sutter Instrument Company, Novato, CA). A motorized progressive filter (Carl Zeiss Canada Ltd., Toronto, Ontario, Canada) was used when measuring excitation spectra between 400 and 600 nm. Fluorescence

was measured with a photomultiplier tube (Hamamatsu Photonics Corp., Bridgewater, NJ) and a 10-nm bandpass filter centered at 589 nm (Omega Optical Inc., Brattleboro, VT). A dichroic mirror with a discrimination wavelength of 570 nm was used (570DCXR, The Optikon Corporation Ltd. Kitchener, Ontario, Canada). A 10-min labelling period was performed on voltage-clamped oocytes at a holding potential of −90 mV using a concentration of 20 μM tetramethylrhodamine-5-maleimide (TMR5M, Molecular Probes, Eugene OR). As autofluorescence was found to be higher at the vegetal pole of the oocyte, all fluorescent experiments were performed using the animal pole. Fluorescence intensity was read at the maximal excitation wavelength.

2.5. Data analysis and statistics

Amino acids sequences were aligned using ClustalX and were displayed using Genedoc ([18], http://www.psc.edu/biomed/genedoc). Experiments with MTS reagents were performed on at least 3 oocytes obtained from a minimum of 2 different donors. Data are reported as mean ± S.E. (except when otherwise noted) and are compared using unpaired Student's *t*-test; statistical significance was set at $p < 0.05$. Curve fitting of current values for determination of both $K_m^{\alpha MG}$ and K_i^{Pz} and statistical tests were performed using Origin 7 (OriginLab Corporation, Northampton, MA).

3. Results

3.1. Effect of MTS reagents

The large inward current through SGLT1 is due to the cotransport of two Na^+ ions along with each αMG molecule into the cell. SGLT1 also displays a Pz-sensitive Na^+ current in the absence of sugar, referred to as a Na^+ leak [19]. The accessibility of cysteine residues introduced into the protein sequence was tested by measuring the effect of non-permeant, Cys-binding reagents (MTSET, MTSES) on the I_{cotr} (maximal αMG cotransport current) and on the I_{leak} (Na^+ leak current).

As the human SGLT1 contains 15 endogenous cysteine residues, it was necessary to begin by characterizing the effects of MTS reagents on the activity of the native cotransporter. Fig. 2 illustrates the current/voltage ($I-V$) relationship of the I_{cotr} and I_{leak} for 6 oocytes before and after treatment with MTSES (panel A) or MTSET (panel B). The currents stimulated by the addition of 5 mM αMG were unaffected by a 5-min treatment with either MTS reagent. On average, the I_{cotr} at −95 mV, after treatment with MTSES or MTSET, represent 95±4% and 107±2% of the pre-treatment currents, respectively (see Fig. 2C, left). The I_{leak} was also found to be insensitive to treatment with MTS reagents; the I_{leak} after MTSES or MTSET treatment averaged 89±7% and 107±7%, respectively, of their

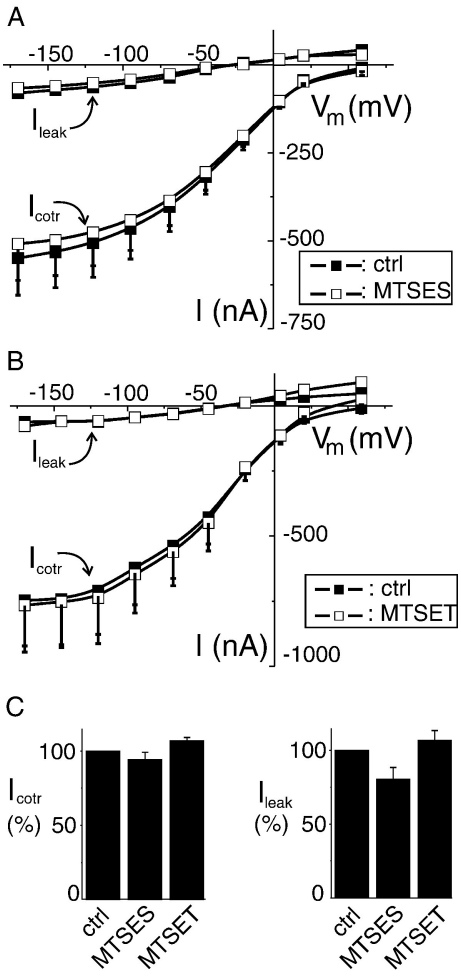

Fig. 2. Effect of MTSES and MTSET treatments on αMG-dependent currents (5 mM) and phlorizin-sensitive Na^+ leak currents of wild type hSGLT1. (A) $I-V$ curve of I_{cotr} and I_{leak} before and after MTSES treatment (paired experiments, $n=6$). (B) $I-V$ curve of I_{cotr} and I_{leak} before and after MTSET treatment (paired experiments, $n=6$). Error bars represent 1 S.E.M. and are shown when larger than symbols. (C) Comparison of currents after MTS treatments to the control currents (set at 100%) at −95 mV for I_{cotr} (left) and I_{leak} (right).

magnitude immediately prior to the treatment (see Fig. 2C, right). These results are in agreement with previously mentioned observations [4,7]. The absence of any significant effects of MTS reagents on oocytes expressing wtSGLT1 indicates that the endogenous cysteine residues are either physically non-accessible, already involved in a disulfide bridge or, alternatively, that they are accessible but that their covalent modification does not produce any significant functional changes in the transport mechanism of the cotransporter.

Amino acids N565, K567, E586, I588, A605, Y606, D607, L608, E624, E625, K626, M630, M632 and T635 were individually replaced by cysteine in SGLT1 cDNA (see Fig. 1B). The C-terminal amino acid (A664) was also replaced with cysteine in order to assess its location. All the mutants exhibited good expression levels as their I_{cotr} (in the presence of 5 mM αMG) ranged from 47% of the wtSGLT1

I_{cotr} (for A664C) to 185% (for M632C) (Fig. 3). The I_{leak} for every mutant was also very similar to that of the wtSGLT1 except for E586C, which had a I_{leak} corresponding to only 30% of the wtSGLT1, and for T635C which had a significantly increased I_{leak} (130% of wtSGLT1 I_{leak}). Consequently, each of the 15 different mutants was suitably folded and inserted in the plasma membrane, leading to reliable, functional expression in *Xenopus* oocytes.

Cotransport and Na^+ leak currents were measured for 3 or 4 oocytes expressing each of these mutants before submitting them to a 5- to 10-min treatment with 2.5 mM MTSES or MTSET. These currents were then re-evaluated and the ratios between currents measured after treatment to initial currents were calculated. The results of the effects of MTSES and MTSET on the individual mutants are summarized in Fig. 4 and are compared to the (statistically insignificant) effects observed with oocytes expressing the wtSGLT1 cotransporter.

Binding of extracellular MTSES or MTSET to the cysteine residues introduced at 9 different locations in loop 13–14 produced a statistically significant effect in the I_{cotr} and/or I_{leak}. The combined effects of MTSES and MTSET established that the following amino acid positions are accessible to the external solution: 565, 567, 588, 605, 624, 625, 632, 635 and 664. One significant effect on mutant E624C is shown in Fig. 5A and B, where the MTSET-induced increase in I_{cotr} (137±9%) was considerable while the same treatment had no significant effect on the I_{leak}. Of the MTS-accessible locations, a few were observed to produce very large effects on the cotransporter functions. For example, the effect of MTSET on A664C was obvious as it increased the I_{cotr} nearly two-fold and decreased the

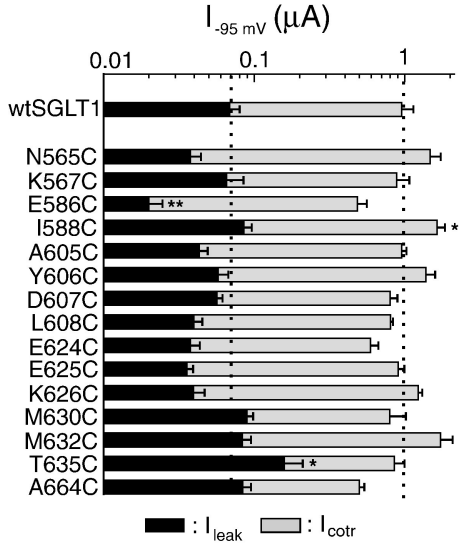

Fig. 3. Comparison of mutated SGLT1 activities to that of wtSGLT1. Maximal αMG cotransport (I_{cotr} at 5 mM αMG) and Na^+ leak (I_{leak}) currents at −95 mV of all the mutants expressed in *Xenopus* oocytes. The dotted lines indicate the mean expression level of wtSGLT1. $n \geq 6$ for each mutant. Errors are S.E.M. and stars indicate the statistical significance with respect to wtSGLT1 (*$P \leq 0.05$, **$P \leq 0.01$, ***$P \leq 0.001$).

I_{leak} by more than 60% (Fig. 5C and D). In the case of K567C, M632C and T635C, the I_{leak} currents were practically doubled (Fig. 4). Despite their charge difference, MTSET and MTSES were never seen to produce opposite effects on any of the mutants studied.

In conclusion, the effects of exposure to MTS reagents indicate that loop 13–14 (AA #549 to 637) can be reached from the extracellular space at, at least, 9 different locations ranging from AA #565 to 635. It should be noted that external accessibility to the other locations tested could have been overlooked if MTSES or MTSET could bind to the cysteine residue without producing any detectable, functional effects on the two electrophysiological parameters tested. It also suggests that these residues are somehow important for SGLT1's function as exposition to a MTS reagent significantly modifies I_{cotr} and/or I_{leak}.

3.2. Labelling with fluorescent probes

In order to complement our accessibility study with a method that does not require observation of an effect on cotransporter function, we used a maleimide-conjugated fluorescent probe to label the cysteine mutants of loop 13–14. With a triangular size of about 14 by 8 Å, as compared to the cylindrical MTS reagents (10 Å long with a diameter of approximately 6 Å [20]), it is expected that the accessibility determined by these two reagents might differ significantly.

Binding of the fluorescent probe to oocytes exposed to 20 μM TMR5M for 10 min was detected by obtaining excitation spectra from 400 to 600 nm. As shown in Fig. 6, the fluorescence measurements performed on the wtSGLT1 and on mutants K567C and E586C reveal maximum absorption at a wavelength of about 560 nm. We performed excitation spectra on every oocyte and used the 560-nm measurement to compare experiments.

With a reading window of 250 μm × 250 μm, our fluorescence set-up yielded a fluorescence signal of 0.24± 0.03 V (n=58) at an excitation wavelength of 560 nm for a non-labelled oocyte. This is considered to derive from the combined autofluorescence originating from the oocyte, from the different optical components and from the bath. When a non-injected oocyte is treated with the standard labelling procedure (see Materials and methods), fluorophore internalisation and endogenous membrane protein labelling yield a total fluorescence signal of 0.5±0.7 V (n=4) (see Table 1). Oocytes expressing the wtSGLT1 generated a fluorescent signal averaging 1.5±0.3 V (n=8) which was higher than the autofluorescence level but not significantly different from the signal obtained from non-injected oocytes exposed to the fluorophore for the same period (P=0.23). This indicates that the 15 endogenous cysteine residues in SGLT1 are inaccessible to the fluorophore, agreeing with the observation above that neither MTSES nor MTSET affected the function of the wtSGLT1 cotransporter. An example of significant labelling is shown

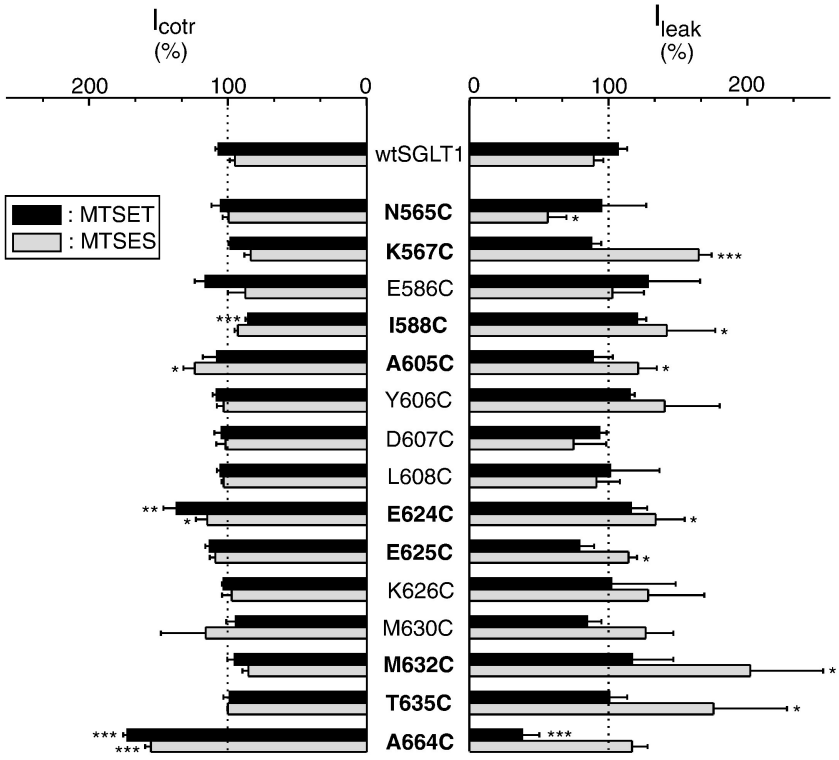

Fig. 4. Effects of MTSES and MTSET on maximal αMG cotransport and Na^+ leak currents of wild type and mutant SGLT1. The currents measured after MTS treatment are depicted as a proportion of the control currents (set at 100%) at −95 mV for I_{cotr} (left) and I_{leak} (right). Black bars are for MTSET and gray bars for MTSES treatments. The dotted line is at 100%. $n=3$ to 4 oocytes for each type of experiment on each mutant, $n=6$ for wtSGLT1. Errors are S.E.M. Stars represent statistical significance vs. wtSGLT1 (as in Fig. 3) and the names of the accessible mutants have been printed in bold characters.

in Fig. 6 for E586C, and the data for all the mutants of the loop and for the last C-terminal amino acid (A664C) are presented in Table 1. Three of the 15 mutants (E586C, I588C and E624C) were shown to be accessible to an extracellular fluorescent probe using our labelling procedure. In addition, pre-treatment with either MTSET or MTSES appeared to be effective in reducing the labelling observed for these mutants to the level obtained with wtSGLT1 (data not shown). The activity of the mutant proteins was unaffected by the binding of the TMR5M reagent, based on substrate-induced currents (data not shown).

3.3. Membrane potential effect on fluorescence

Fluorescent labelling of the mutant Q457C was previously shown to produce a fluorescent signal that can be affected by ligands and voltage-dependent conformational changes of the protein [5]. We confirmed this result by observing that, from +50 to −150 mV, the fluorescent signal for this mutant changed by 4–5% (data not shown). Unfortunately, for mutants presenting significant fluorescent labelling (E586C, I588C and E624C), none displayed a voltage sensitivity that exceeded the noise level of 0.5%. This was repeated in the presence of 5 mM αMG but no voltage-dependent fluorescence change could be observed (data not shown).

3.4. Affinities for substrate and inhibitor

As Novakova et al. [12], Raja et al. [14] and Xia et al. [13] have proposed that the region between amino acids 604 and 610 in rSGLT1 appeared to be involved in the Pz binding site, we measured the apparent affinity for αMG ($K_m^{\alpha MG}$) and the inhibition constant for Pz (K_i^{Pz}) of mutant SGLT1 versions with cysteine residues inserted into this region. Fig. 7A illustrates the absence of voltage dependence for these affinities measured with the wtSGLT1. All the affinities of the mutants tested were likewise insensitive to membrane potential, so affinities were compared at −150 mV (Fig. 7B) for 4 mutants within the proposed Pz binding site (A605C, Y606C, D607C and L608C) and for 2 flanking mutants in loop 13–14 (I588C, E625C). This membrane potential was chosen because of the well defined affinity for Na^+ (15 mM) at this voltage. The $K_m^{\alpha MG}$ of wtSGLT1 is 0.9±0.1 mM (at −150 mV) and the mutants displayed values which were not statistically different from this, aside from mutant D607C which exhibited greater affinity (0.51±0.04 mM). However, the K_i^{Pz} for 3 of the mutants were significantly higher than for the wtSGLT1 (see Fig. 7B). As the binding of αMG is dependent on prior Na^+ binding, any change in K_m^{Na+} should foster a change in $K_m^{\alpha MG}$. Consequently, as the Na^+ dependent $K_m^{\alpha MG}$ of mutants is not different from that of wtSGLT1, the change in

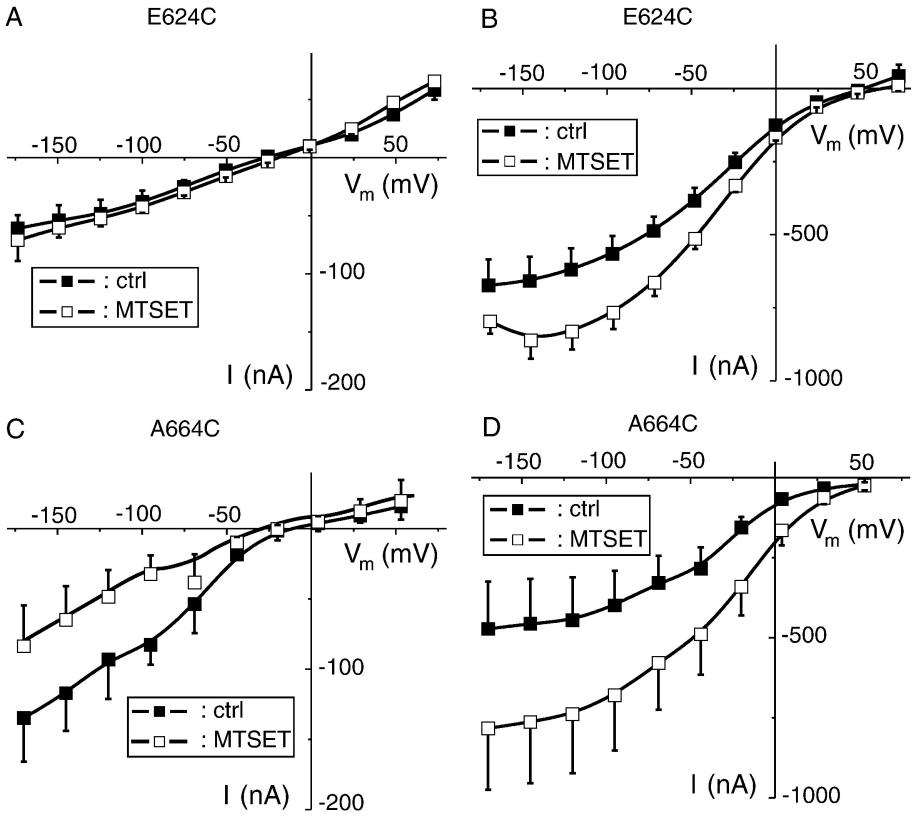

Fig. 5. Effect of MTSET treatment on maximal αMG (5 mM) cotransport and Na^+ leak currents for mutants E624C and A664C. (A) $I-V$ curve of I_{leak} before and after MTSET treatment for mutant E624C ($n=3$, paired experiments). (B) $I-V$ curve of I_{cotr} before and after MTSET treatment for mutant E624C ($n=3$, paired experiments). (C) $I-V$ curve of I_{leak} before and after MTSET treatment for mutant A664C ($n=3$, paired experiments). (D) $I-V$ curve of I_{cotr} current before and after MTSET treatment for mutant A664C ($n=3$, paired experiments). Errors are S.E.M.

the K_i^{Pz} of the mutant SGLT1s is not likely to be due to a change in K_m^{Na+}.

4. Discussion

The substituted cysteine accessibility method (SCAM) has proven to be a useful tool for examining the accessibility and role of specific membrane protein segments [21–23]. Experimental results, in combination with molecular modelling, can help to refine established models for protein structures, as was done for the Ca^{2+}-activated K^+ channel [24] and ECaC-TRPV5 [25] models, or to understand permeation mechanisms in other types of transporters [26–29]. In the absence of crystal structure, these data could lead to major advances in the understanding of molecular mechanisms of action of transport proteins [30–33].

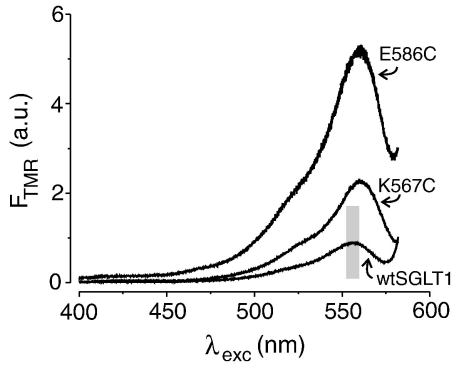

Fig. 6. Excitation spectra of representative oocytes expressing wtSGLT1, K567C and E586C, labelled with TMR5M. Fluorescence is quantitated in arbitrary units. The grey box represents ±1 S.D. for the non-specific labelling measured on the wtSGLT1.

4.1. MTS results

We chose not to produce a cysteine-less cotransporter before doing SCAM for two reasons. First, neither MTSES nor MTSET had any functional effects on wtSGLT1 and its labelling with TMR5M was not different than the labelling of non-injected oocytes. Second, we knew that replacing cysteines at positions 560 or 610 would affect the kinetics of SGLT1 (data not shown) and it would be meaningless to study the accessibility of a specific loop in a structurally challenged cotransporter. Other studies using SCAM have also used a wild-type transporter instead of a cysteine-less version because of the deleterious effects of removing cysteines from the protein [32,34–37].

Table 1
Fluorescent labelling of the mutants in loop 13–14 with a rhodamine-based fluorophore (TMR5M)

Mutant	Intensity[a] (a.u.)	*t*-test[b]	*n*[c]	Accessibility[d]
N.I.[e]	0.5±0.7	0.23	4	
wtSGLT1	1.5±0.3	–	8	
N565C	3±1	0.20	6	–
K567C	1.8±0.9	0.64	3	–
E586C	3.6±0.6	0.003	4	x
I588C	3.6±0.7	0.05	4	x
A605C	3±3	0.20	4	–
Y606C	0.54±0.08	0.05	4	–
D607C	2±1	0.37	3	–
L608C	3±2	0.14	3	–
E624C	6±1	0.001	4	x
E625C	0.7±0.3	0.14	4	–
K626C	1.9±0.7	0.49	4	–
M630C	3±2	0.16	3	–
M632C	1.1±0.3	0.41	4	–
T635C	2±1	0.58	4	–
A664C	1.1±0.4	0.48	3	–

[a] Each entry is the mean±SEM of the maximum fluorescent signal taken from the excitation spectrum for each labelled oocyte (see Materials and methods and Fig. 6).
[b] t-test entries represent the p value for unpaired Student's *t*-test against wtSGLT1 data.
[c] *n* is the number of experiments.
[d] A significant labelling of a mutant as compared to wtSGLT1 is identified by x and no accessibility to the fluorescent probe by –.
[e] Non-injected oocyte.

An unambiguous observation from MTS reagent labelling is that cysteine residues inserted in 9 different positions within loop 13–14 are accessible from the external solution by MTSET and/or MTSES. In the present study, MTSES was found to be more potent than MTSET. Six mutants were exclusively sensitive to MTSES (N565C, K567C, A605C, E625C, M632C and T635C), 3 mutants were affected by both MTSES and MTSET and none of the mutants was exclusively affected by MTSET. In the 3 cases, where both MTS reagents were effective, the effects do not appear to be charge-related as MTSET and MTSES do not simply have opposite effects on the parameter measured. In addition, an effect on I_{cotr} was not systematically accompanied by an effect on the I_{leak}. We can deduce from the MTS results that the amino acids in positions 565, 567, 588, 605, 624, 625, 632 and 635 within the last hydrophilic loop are hydrated and accessible from the extracellular medium by small hydrophilic compounds like MTSES and MTSET. We also assessed the accessibility of the C-terminus amino acid, A664, as both MTSES and MTSET affected transport through the A664C mutant.

4.2. Fluorescent labelling

Introducing cysteine into positions 586, 588 or 624 allowed significant binding of the fluorescent agent TMR5M, which could be prevented by pre-exposure to MTS reagents. While the cysteines inserted into positions 588 and 624 were shown to be affected by exposure to MTS reagents (see Figs. 4 and 5), transport through the mutant E586C was not affected by the MTS reagent although the mutant protein was clearly labelled with TMR5M in the absence of the MTS reagent. This appears to be a situation where the MTS reagent binds to the cysteine residue without perturbing SGLT1 function. In the 7 other cases presented in Fig. 4, MTS reagents could reach the cysteine residues but the fluorophore could not. This could indicate that access to the cysteine residue is limited such that a molecule the shape of the fluorophore used could not reach this position. It should also be recalled that, as the fluorescent probe is maleimide based, it could react differently than do the MTS reagents.

4.3. Affinities for αMG and Pz

Amino acids 604–610 of rSGLT1 have been proposed to be important for Pz binding based on changes in K_i^{Pz}, but not in $K_m^{\alpha MG}$, of lysine mutants of the complete rSGLT1 protein expressed in COS-7 cells [12]. However, the most convincing results supporting this proposal were obtained

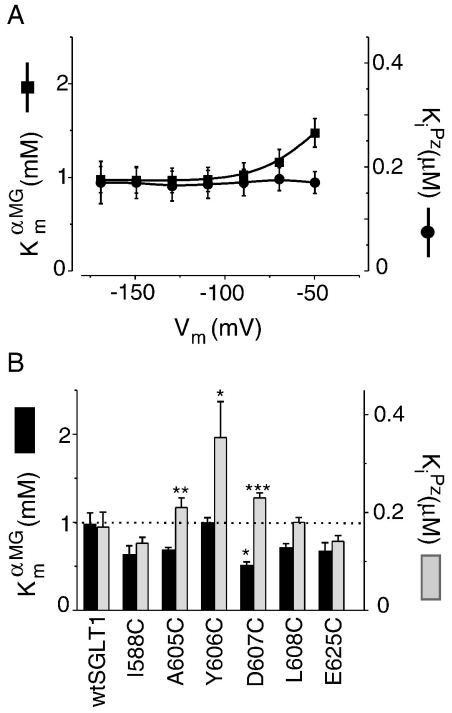

Fig. 7. Apparent affinity for αMG and apparent inhibition constant of Pz for some selected mutants, compared to wtSGLT1. (A) Voltage dependency of apparent αMG affinity ($K_m^{\alpha MG}$) and apparent Pz inhibition constant (K_i^{Pz}) for wtSGLT1. Filled squares represent $K_m^{\alpha MG}$, filled circles represent K_i^{Pz}. (B) $K_m^{\alpha MG}$ and K_i^{Pz} measured at −150 mV for wtSGLT1 and for some selected mutants in loop 13–14. Black bars represent $K_m^{\alpha MG}$, grey bars represent K_i^{Pz}. The dotted line indicates the levels of $K_m^{\alpha MG}$ and K_i^{Pz} for wtSGLT1. $n \geq 4$. The stars depicting statistical significance are as described for Fig. 3.

using mutated version of the isolated and purified loop 13–14 rather than intact SGLT1. Raja et al. [14] and Xia et al. [13] have observed that Pz can bind to this loop in situ (with K_d values similar to that seen with the wild-type isolated loop, ranging from 15 to 26 μM) and changed the fluorescence quenching (Trp fluorescence) of the mutated isolated loop which had the modified putative Pz binding site (D611W had a K_d of 54 μM). In our study, only mutant D607C exhibited a significant change in $K_m^{\alpha MG}$, but 3 mutants in the putative Pz site had a different K_i^{Pz}. The sequence AYDL (positions 605–608) is conserved between SGLT1 and SGLT3 but is replaced by CLLW in SGLT2, which is also Pz sensitive but with a higher K_i than SGLT1 (9 μM at −50 mV in pSGLT2, measured by electrophysiology using SGLT2 expressed in *Xenopus* oocytes) [38]. It is interesting that our study using the whole cotransporter revealed that a cysteine introduced to replace any of the normal A, Y or D residues produced a significant increase in the Pz K_i. While confirming the possible interaction between this segment and Pz, it seems that mutation to cysteine produces very little change, indicating that the geometry of AYDL is not a crucial element in favouring Pz binding.

4.4. Topology in the last TMS

The presently accepted topologic model of the Na^+/glucose cotransporter has progressively evolved [39] since the cloning of the cotransporter. An N-glycosylation insertion site study helped to test the orientation of most of the previously proposed 12 TMS [1], confirming certain TMS orientations and adding one TMS near the N-terminus and another at the C-terminus. Since that time, some evidence has arisen to challenge the assigned topology of the C-terminal region of the protein [11].

Fig. 8 illustrates the experimental evidence underlying the topologic model of the last 4 TMS. For TMS XI to XIII, the first experimental evidence supporting the topologic model is that amino acid Q457 can be mutated into a cysteine which can be reached and altered by MTSES, MTSET and MTSEA or labelled with TMR6M (Fig. 8, position a) [4,5]. A subsequent glycosylation scanning study found that insertion of a glycosylation site at position 518 resulted in a functional, glycosylated transporter indicating that this sequence was facing the extracellular medium (Fig. 8, position b) [1].

The topology of loop 13–14 has been directly or indirectly tested using several different methods but contradictory results have been obtained. Insertion of a glycosylation site into loop 13–14 resulted in a non-functional protein [1], possibly due to the difficulties of inserting such a long segment (42 amino acids) without affecting the protein structure. Using ultra-thin frozen sections of rat kidney, immunohistochemical localization of SGLT1 with gold particles and a specific antibody recognizing amino acids 564 to 575 suggested an intracellular location for this

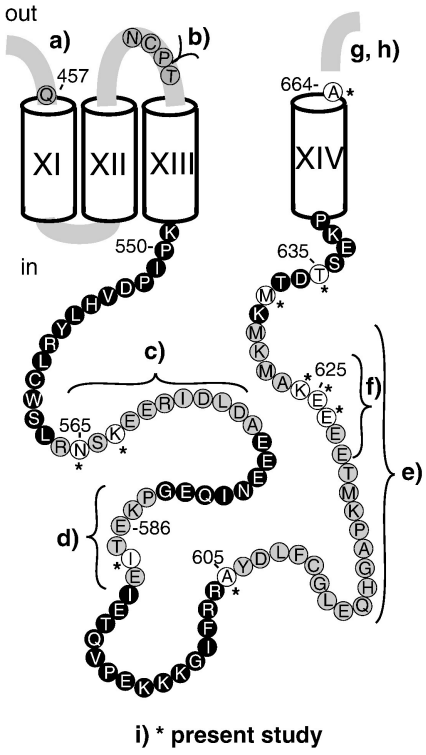

Fig. 8. Summary of experimental results from the present study and from other publications regarding accessibility of the last 4 transmembrane segments. TMS are identified by Roman numerals, numbers indicating position in the human SGLT1 protein sequence are shown and the extracellular and intracellular side are indicated by the words "out" and "in", respectively. (a) The residue Q457 is accessible from the extracellular medium to both MTS reagents and to the TMR6M fluorescent probe [5]. (b) Insertion of an N-glycosylation site at position 518 produced a functional mutant and the amino acid residue was glycosylated, suggesting the accessibility of the site from the extracellular milieu [1]. (c) An antibody recognizing an epitope of amino acids 564 to 575 localized this epitope at the cytoplasmic surface of the membrane in rat kidney sections [40]. (d), (e), and (f) Two 6-His mutants (from 584 to 589 and from 622 to 627) were functional and labelled by an antibody in non-permeabilized COS-7 cells, and an antibody recognizing an epitope from AA 606 to 630 in non-permeabilized COS-7 cells suggested an extracellular location [11]. (g) 6-His extension functional mutant (position 662) was observed in permeabilized cells, suggesting intracellular location [11]. (h) An antibody directed against a VSVG tag added to the C-terminus of rSGLT1 recognized its epitope in permeabilized Caco-2 cells only, also suggesting intracellular location [41]. (i) Accessible residues examined in this study are shown in white with stars.

epitope in SGLT1 (Fig. 8, position c) [40]. Insertion of a polyhistidine tag by Kinne's lab [11] indicated that the protein region between amino acids 584 and 630 should be extracellular. A major drawback of this study is that 7 of the 11 mutants were nonfunctional, which precludes their use in ascertaining the membrane topology of correctly folded (i.e., active) SGLT1. Of the 4 functional mutants, 2 showed that positions 584–589 and positions 622–627 were located extracellularly (Fig. 8, positions d and f). Some other SGLT1 peptide sequences were also used in the same study to create specific, epitope-directed antibodies against wtSGLT1 expressed in CHO cells. These results confirmed

the topology of regions 306–311 (intracellular), 336–356 (extracellular) and 402–407 (intracellular) in SGLT1. The present study shows 15 cysteine mutants, all functional, of which amino acids 565, 567, 586, 588, 605, 624, 625, 632 and 635 in loop 13–14 (was after being mutated into a cysteine) could be reached by hydrophilic MTS reagents and/or by a fluorophore added in the extracellular solution. This indicates that cysteine substitution creates less perturbation in SGLT1 structure than does 6-His insertion. For several of our Cys substitutions, additional credibility is provided by obtaining evidence of accessibility by the use of two different procedures. Our results with loop 13–14 are globally in accordance with the results from Kinne's lab [11] but contradict the intracellular immunohistochemical localization of residues 564–575 using kidney section [40].

A few studies have attempted to experimentally determine the orientation of the C-terminus in SGLT1. Turner et al. [41] successfully expressed a VSVG-tagged rSGLT1 in Cos-1 and Caco-2 cells. Unfortunately, the protein did exhibited severely attenuated transport, suggesting an functionally important conformational change. In addition, the protein was mistargeted to the basolateral membrane. As the anti-VSVG antibody required cell permeabilization to yield significant labelling, it was concluded that the C-terminus was facing the intracellular milieu (Fig. 8, position h). The position of the C-terminus was also deduced to be either intracellular or to be part of the transmembrane domain following addition of a 6-His tag at position 662, observed in permeabilized COS-7 cells (Fig. 8, position g) [11]. Unfortunately, in *Xenopus* oocytes, this result could not be confirmed using another tag as addition of myc, HA or poly-His tags to the C-terminus did not produce a functional cotransporter [15]. Overall, the exact location of the C-terminus is not well established. The addition of a tag at the C-terminus could itself affect the membrane insertion of the last TMS, as apparently happened with insertion of an N-glycosylation sequence at the N-terminus [1]. We have shown that both MTSES and MTSET increased the I_{leak} by about 50% and that MTSET reduced the I_{cotr} by almost 60% for mutant A664C. We thus conclude that a cysteine residue in position 664 is accessible from the extracellular medium. As a single amino acid substitution is likely to have less of an effect on the topology of the C-terminal region than would a hexapeptide insertion, the present study provides an additional support to the contention that the C-terminus of SGLT1 is facing the extracellular milieu.

4.5. The hypothesis of a re-entrant loop

As discussed above, strong evidence supports the orientation of TMS XIII as shown in Fig. 8 and, despite some contradictory interpretations, the present study suggests that the C-terminus of TMS XIV is extracellular. This would indicate that loop 13–14 would start and finish at the intracellular side and could form some kind of re-entrant loop, allowing accessibility from the extracellular solution. Recently obtained crystal structures of different cotransporters and channels indicate that, in several instances, membrane-interacting short helices were not correctly predicted from hydropathy profiles [10,42–44]. One peculiarity of loop 13–14 is its considerable hydrophilicity, which would normally preclude any membrane-interacting configuration for this segment. This feature, and the ambiguous membrane orientation of this highly charged loop which is indicated by the present study, are reminiscent of the voltage-sensor (S4 segment) of voltage-dependent ion channels, whose transmembrane orientation remains controversial [45–48].

In summary, immunolocalization, using peptide-specific antibodies or peptide tags [11], and the MTS accessibility results presented in this study are not consistent with the membrane topology proposed in 1996 [1] as shown in Fig. 8. Some experimental evidence has been shown to confirm the orientations of TMS XI and TMS XIII [1,4] but the orientation of the last TMS remains ambiguous ([1,11,41], this study). As the long "intracellular" loop 13–14 appears to be accessible from the external solution, at least at positions 565–589 and 605–635, and as MTS reagents can affect the functions of some mutant, this interesting loop may form a re-entrant loop or else be exposed at both surfaces, either simultaneously or at different points during the transport cycle.

Acknowledgements

We would like to express our gratitude to Michel Brunette for technical assistance and help with experimental setup. This work was supported by the Canadian Institutes of Health Research (grant #MOP-10580). D.G.G. is a NSERC and FRSQ postgraduate scholar.

References

[1] E. Turk, C.J. Kerner, M.P. Lostao, E.M. Wright, Membrane topology of the human Na+/glucose cotransporter SGLT1, J. Biol. Chem. 271 (1996) 1925–1934.
[2] M. Panayotova-Heiermann, S. Eskandari, E. Turk, G.A. Zampighi, E.M. Wright, Five transmembrane helices form the sugar pathway through the Na+/glucose cotransporter, J. Biol. Chem. 272 (1997) 20324–20327.
[3] M. Panayotova-Heiermann, E.M. Wright, Mapping the urea channel through the rabbit Na(+)-glucose cotransporter SGLT1, J. Physiol. 535 (2001) 419–425.
[4] D.D. Loo, B.A. Hirayama, E.M. Gallardo, J.T. Lam, E. Turk, E.M. Wright, Conformational changes couple Na+ and glucose transport, Proc. Natl. Acad. Sci. U. S. A. 95 (1998) 7789–7794.
[5] A.K. Meinild, B.A. Hirayama, E.M. Wright, D.D. Loo, Fluorescence studies of ligand-induced conformational changes of the Na(+)/glucose cotransporter, Biochemistry 41 (2002) 1250–1258.
[6] S.A. Huntley, D. Krofchick, M. Silverman, Position 170 of rabbit Na+/glucose cotransporter (rSGLT1) lies in the Na+ pathway;

modulation of polarity/charge at this site regulates charge transfer and carrier turnover, Biophys. J. 87 (2004) 295–310.
[7] B. Lo, M. Silverman, Cysteine scanning mutagenesis of the segment between putative transmembrane helices IV and V of the high affinity Na+/Glucose cotransporter SGLT1. Evidence that this region participates in the Na+ and voltage dependence of the transporter, J. Biol. Chem. 273 (1998) 29341–29351.
[8] B. Lo, M. Silverman, Replacement of Ala-166 with cysteine in the high affinity rabbit sodium/glucose transporter alters transport kinetics and allows methanethiosulfonate ethylamine to inhibit transporter function, J. Biol. Chem. 273 (1998) 903–909.
[9] S. Vayro, B. Lo, M. Silverman, Functional studies of the rabbit intestinal Na+/glucose carrier (SGLT1) expressed in COS-7 cells: evaluation of the mutant A166C indicates this region is important for Na+-activation of the carrier, Biochem. J. 332 (Pt. 1) (1998) 119–125.
[10] J. Abramson, I. Smirnova, V. Kasho, G. Verner, H.R. Kaback, S. Iwata, Structure and mechanism of the lactose permease of *Escherichia coli*, Science 301 (2003) 610–615.
[11] J. Lin, J. Kormanec, D. Homerova, R.K. Kinne, Probing transmembrane topology of the high-affinity sodium/glucose cotransporter (SGLT1) with histidine-tagged mutants, J. Membr. Biol. 170 (1999) 243–252.
[12] R. Novakova, D. Homerova, R.K. Kinne, E. Kinne-Saffran, J.T. Lin, Identification of a region critically involved in the interaction of phlorizin with the rabbit sodium-D-glucose cotransporter SGLT1, J. Membr. Biol. 184 (2001) 55–60.
[13] X. Xia, J.T. Lin, R.K. Kinne, Binding of phlorizin to the isolated C-terminal extramembranous loop of the Na+/glucose cotransporter assessed by intrinsic tryptophan fluorescence, Biochemistry 42 (2003) 6115–6120.
[14] M.M. Raja, N.K. Tyagi, R.K. Kinne, Phlorizin recognition in a C-terminal fragment of SGLT1 studied by tryptophan scanning and affinity labeling, J. Biol. Chem. 278 (2003) 49154–49163.
[15] P. Bissonnette, J. Noel, M.J. Coady, J.Y. Lapointe, Functional expression of tagged human Na+-glucose cotransporter in *Xenopus laevis* oocytes, J. Physiol. 520 (Pt. 2) (1999) 359–371.
[16] C.L. Fisher, G.K. Pei, Modification of a PCR-based site-directed mutagenesis method, Biotechniques 23 (1997) 570–571 (574).
[17] M.P. Gagnon, P. Bissonnette, L.M. Deslandes, B. Wallendorff, J.Y. Lapointe, Glucose accumulation can account for the initial water flux triggered by Na+/glucose cotransport, Biophys. J. 86 (2004) 125–133.
[18] J.D. Thompson, T.J. Gibson, F. Plewniak, F. Jeanmougin, D.G. Higgins, The CLUSTAL_X windows interface: flexible strategies for multiple sequence alignment aided by quality analysis tools, Nucleic Acids Res. 25 (1997) 4876–4882.
[19] L. Parent, S. Supplisson, D.D. Loo, E.M. Wright, Electrogenic properties of the cloned Na+/glucose cotransporter: I. Voltage-clamp studies, J. Membr. Biol. 125 (1992) 49–62.
[20] A. Fabiato, F. Fabiato, Calculator programs for computing the composition of the solutions containing multiple metals and ligands used for experiments in skinned muscle cells, J. Physiol. (Paris) 75 (1979) 463–505.
[21] S. Jung, M.H. Akabas, R.A. Harris, Functional and structural analysis of the GABAA receptor a1 subunit during channel gating and alcohol modulation, J. Biol. Chem. 280 (2004) 308–316.
[22] A. Karlin, M.H. Akabas, Substituted-cysteine accessibility method, Methods Enzymol. 293 (1998) 123–145.
[23] C. Ehnes, I.C. Forster, K. Kohler, A. Bacconi, G. Stange, J. Biber, H. Murer, Structure-function relations of the first and fourth predicted extracellular linkers of the type IIa Na+/Pi cotransporter: I. Cysteine scanning mutagenesis, J. Gen. Physiol. 124 (2004) 475–488.
[24] M. Simoes, L. Garneau, H. Klein, U. Banderali, F. Hobeila, B. Roux, L. Parent, R. Sauve, Cysteine mutagenesis and computer modeling of the S6 region of an intermediate conductance IKCa channel, J. Gen. Physiol. 120 (2002) 99–116.
[25] Y. Dodier, U. Banderali, H. Klein, O. Topalak, O. Dafi, M. Simoes, G. Bernatchez, R. Sauve, L. Parent, Outer pore topology of the ECaC-TRPV5 channel by cysteine scan mutagenesis, J. Biol. Chem. 279 (2004) 6853–6862.
[26] N. Chakrabarti, B. Roux, R. Pomes, Structural determinants of proton blockage in aquaporins, J. Mol. Biol. 343 (2004) 493–510.
[27] T.W. Allen, O.S. Andersen, B. Roux, Energetics of ion conduction through the gramicidin channel, Proc. Natl. Acad. Sci. 101 (2004) 117–122.
[28] S.Y. Noskov, W. Im, B. Roux, Ion permeation through the {alpha}-hemolysin channel: theoretical studies based on Brownian dynamics and Poisson–Nernst–Plank electrodiffusion theory, Biophys. J. 87 (2004) 2299–2309.
[29] Y. Arinaminpathy, P.C. Biggin, I.H. Shrivastava, M.S.P. Sansom, A prokaryotic glutamate receptor: homology modelling and molecular dynamics simulations of GluR0, 553 (2003) 321.
[30] H.R. Kaback, M. Sahin-Toth, A.B. Weinglass, The kamikaze approach to membrane transport, Nat. Rev., Mol. Cell Biol. 2 (2001) 610–620.
[31] G. Lambert, I.C. Forster, G. Stange, K. Kohler, J. Biber, H. Murer, Cysteine mutagenesis reveals novel structure–function features within the predicted third extracellular loop of the type IIa Na(+)/P(i) cotransporter, J. Gen. Physiol. 117 (2001) 533–546.
[32] X. Yao, A.M. Pajor, Arginine-349 and aspartate-373 of the Na(+)/dicarboxylate cotransporter are conformationally sensitive residues, Biochemistry 41 (2002) 1083–1090.
[33] A.M. Pajor, Conformationally sensitive residues in transmembrane domain 9 of the Na+/dicarboxylate co-transporter, J. Biol. Chem. 276 (2001) 29961–29968.
[34] A.M. Pajor, S.J. Krajewski, N. Sun, R. Gangula, Cysteine residues in the Na+/dicarboxylate co-transporter, NaDC-1, Biochem. J. 344 (Pt. 1) (1999) 205–209.
[35] G. Lambert, I.C. Forster, J. Biber, H. Murer, Cysteine residues and the structure of the rat renal proximal tubular type II sodium phosphate cotransporter (rat NaPi IIa), J. Membr. Biol. 176 (2000) 133–141.
[36] K. Kohler, I.C. Forster, G. Stange, J. Biber, H. Murer, Essential cysteine residues of the type IIa Na+/Pi cotransporter, Pflugers Arch. 446 (2003) 203–210.
[37] C. Ehnes, I.C. Forster, K. Kohler, A. Bacconi, G. Stange, J. Biber, H. Murer, Structure–function relations of the first and fourth predicted extracellular linkers of the type IIa Na+/Pi cotransporter: I. Cysteine scanning mutagenesis, J. Gen. Physiol. 124 (2004) 475–488.
[38] B. Mackenzie, D.D. Loo, M. Panayotova-Heiermann, E.M. Wright, Biophysical characteristics of the pig kidney Na+/glucose cotransporter SGLT2 reveal a common mechanism for SGLT1 and SGLT2, J. Biol. Chem. 271 (1996) 32678–32683.
[39] E. Turk, E.M. Wright, Membrane topology motifs in the SGLT cotransporter family, J. Membr. Biol. 159 (1997) 1–20.
[40] K. Takata, T. Kasahara, M. Kasahara, O. Ezaki, H. Hirano, Localization of Na(+)-dependent active type and erythrocyte/HepG2-type glucose transporters in rat kidney: immunofluorescence and immunogold study, J. Histochem. Cytochem. 39 (1991) 287–298.
[41] J.R. Turner, W.I. Lencer, S. Carlson, J.L. Madara, Carboxy-terminal vesicular stomatitis virus G protein-tagged intestinal Na+-dependent glucose cotransporter (SGLT1): maintenance of surface expression and global transport function with selective perturbation of transport kinetics and polarized expression, J. Biol. Chem. 271 (1996) 7738–7744.
[42] R. Dutzler, E.B. Campbell, M. Cadene, B.T. Chait, R. MacKinnon, X-ray structure of a ClC chloride channel at 3.0 A reveals the molecular basis of anion selectivity, Nature 415 (2002) 287–294.
[43] D.L. Foster, M. Boublik, H.R. Kaback, Structure of the lac carrier protein of *Escherichia coli*, J. Biol. Chem. 258 (1983) 31–34.
[44] D.F. Savage, P.F. Egea, Y. Robles-Colmenares, J.D. O'Connell 3rd, R.M. Stroud, Architecture and selectivity in aquaporins: 2.5 a X-ray structure of aquaporin Z, PLoS Biol. 1 (2003) E72.
[45] M. Laine, D.M. Papazian, B. Roux, Critical assessment of a proposed model of Shaker, FEBS Lett. 564 (2004) 257–263.

[46] M. Laine, M.C. Lin, J.P. Bannister, W.R. Silverman, A.F. Mock, B. Roux, D.M. Papazian, Atomic proximity between S4 segment and pore domain in Shaker potassium channels, Neuron 39 (2003) 467–481.
[47] Y. Jiang, A. Lee, J. Chen, V. Ruta, M. Cadene, B.T. Chait, R. MacKinnon, X-ray structure of a voltage-dependent K+ channel, Nature 423 (2003) 33–41.
[48] Y. Jiang, V. Ruta, J. Chen, A. Lee, R. MacKinnon, The principle of gating charge movement in a voltage-dependent K+ channel, Nature 423 (2003) 42–48.